



## ***Ab initio* study of doping effects in the 42214 compounds: A new family of layered iron-based superconductors**

F. Bucci,<sup>1,\*</sup> A. Sanna,<sup>2</sup> G. Profeta,<sup>3</sup> A. Continenza,<sup>1</sup> and E. K. U. Gross<sup>2</sup>

<sup>1</sup>*Department of Physical and Chemical Sciences, Università di L'Aquila, 67010 Coppito (L'Aquila), Italy*

<sup>2</sup>*Max-Planck-Institut für Mikrostrukturphysik, Weinberg 2, D-06120 Halle, Germany*

<sup>3</sup>*Department of Physical and Chemical Sciences and SPIN-CNR, Università di L'Aquila, 67010 Coppito (L'Aquila), Italy*

(Received 18 October 2016; published 12 January 2017)

We present a systematic DFT-GGA theoretical characterization of the  $\text{RE}_4\text{Fe}_2\text{As}_2\text{Te}_{1-x}\text{O}_{4-y}\text{F}_y$  family of compounds (conventionally called 42214) as a function of a set of key tuning parameters: rare earth (RE = Pr, Sm, and Gd), Te content, oxygen  $\rightarrow$  fluorine substitutional doping, and external pressure. We focus our discussion on the effect of these parameters on magnetic stability and on the nonmagnetic electronic structure, as most relevant aspects related to the occurrence of superconductivity. To uncover the complexity of the 42214 crystal structure, the electronic analysis is based on an unfolding procedure that allows us to observe the behavior of the hole and electron pockets of the Fermi surface and of the nesting function. We complete the present study with the characterization of a related hypothetical compound having Se substituting for Te. Our results show that this peculiar compound family offers very good opportunities to properly harness material properties; based on our results, we infer that suitably tuning a variety of parameters, as those examined here, improved superconducting properties could be achieved.

DOI: [10.1103/PhysRevB.95.014415](https://doi.org/10.1103/PhysRevB.95.014415)

### I. INTRODUCTION

The discovery [1] of superconductivity in fluorine doped iron arsenide  $\text{LaFeAsO}_{1-y}\text{F}_y$  with a critical temperature ( $T_C$ ) of 43 K has triggered an intense scientific investigation on what became a family of Fe-based superconductors [2–6]. Several structural subfamilies have been discovered and great progress was achieved in tuning  $T_C$  by acting with chemical substitution, doping, vacancies, or pressure reaching relatively high values of  $T_C \simeq 50$ –60 K [4]. From these previous works, Katrych and co-workers recently synthesized a new family of Fe-based superconductors with the following general chemical formula:  $\text{RE}_4\text{Fe}_2\text{As}_2\text{Te}_{1-x}\text{O}_{4-y}\text{F}_y$  (42214), where RE is the rare earth element (RE = Pr, Sm, and Gd),  $x$  is the percentage of native tellurium vacancies, and  $y$  is the fluorine content present in the O sites [7,8]. It is experimentally observed that the contraction of the RE covalent radius (moving from Pr to Gd) causes structural modifications that are not sufficient to sensibly raise the critical superconducting temperature which results to be nearly constant ( $T_C \simeq 25$  K) in the 42214 series with different RE atoms (RE = Pr, Sm, and Gd) and approximately similar Te content ( $1 - x \simeq 88\%$ ,  $92\%$ , and  $90\%$  for Pr, Sm, and Gd compounds, respectively) [7]. Nevertheless, as shown by Katrych and co-workers the fluorine substitution of oxygen combined with the presence of native Te vacancies allow us to raise the  $T_C$  up to 45 K (40 K) in the presence of Gd (Sm) [8]. However, experimental measurements emphasize that the synthesized 42214 samples are not optimally doped and it is not absolutely clear if the maximum  $T_C$  has been yet obtained from this new family of Fe-based compounds. Moreover, recent transport measurements on the Pr-based compound, highlight the complexity of these compounds with carriers contributed by different bands and

depending on Te content [9]. Consequently, it is of prior importance to investigate how the electronic properties of 42214 compounds are affected by rare earth atom (RE), Te vacancies ( $x$ ), and fluorine content ( $y$ ) and to understand if their optimal combination could improve the superconductive properties of these new materials. Owing to the structural complexity of this family, theoretical investigations are, so far, very limited. In a previous work [10] we investigated the effect of RE substitution and, to a lesser extent, the structural role of Te vacancies, observing a correlation between magnetic stability and RE size without addressing, however, the main issue regarding the electronic effects of vacancies and doping.

In the large family of high- $T_C$  superconductors, various compounds show many structural and chemical similarities which can be tailored to optimize their physical properties. For example, the 42214 materials seem to share the same building blocks of the 1111 compounds, namely FeAs layers intercalated by oxide RE-O planes: however, in this case they are separated by tellurium spacer planes that add new structural and electronic degree of freedom (for example, by means of chemical substitution) to tune the correlations between structural, magnetic, electronic, and superconductive properties.

Nowadays, the available experimental information on 42214 compounds are still complicated by a nontrivial interplay between the effects of native Te vacancies and fluorine atoms in O sites, which hinder a clear and exhaustive knowledge of the parent 42214 material.

Density functional theory (DFT) calculations in the local density approximation, not residing on any experimental inputs (except crystal structure and chemical composition), can strongly help the comprehension of the structural, electronic, and magnetic properties of this new class of compounds. In this paper we investigate, by means of first-principles DFT calculations, the effect of native Te vacancies, those of fluorine atoms in O sites, as well as the effect of pressure and of Se substitutions.

\*Present address: Scuola Normale Superiore, Piazza dei Cavalieri 7, 56126 Pisa, Italy.

We anticipate that our *ab initio* results give important clues on how to improve the physical properties of these new materials and possibly increase their critical superconducting temperature; moreover, analyzing compound characteristics as As height from the iron plane, magnetic stability, and electronic states at the Fermi level we find important correlations that allow us to improve the scenario described in our previous theoretical work focused on the pure stoichiometric ( $x = 0.0$ ) 42214 materials [10]. Finally, we hope that the present theoretical work will stimulate further experimental work aimed at testing our predictions and at determining the main mechanisms that drive the sought-after material properties.

In the following, we will discuss first-principles results of the 42214 compounds as a function of the Te content outlining their structural, magnetic (Sec. III A), and electronic (Sec. III B) properties at equilibrium and under applied external pressure (Sec. III C). The effect of chemical substitution of oxygen with fluorine is then discussed for RE = Gd (Sec. III D). Finally, we will analyze the physical properties of a set of similar compounds, namely the  $\text{RE}_4\text{Fe}_2\text{As}_2\text{Se}_{1-x}\text{O}_4$  (RE = Pr, Sm, and Gd) where tellurium is fully substituted by selenium (Sec. IV).

## II. COMPUTATIONAL DETAILS

The first-principles calculations were performed using the Vienna *ab initio* simulation package (VASP) [11,12] within the generalized gradient approximation (GGA) [13] to density functional theory. We used projected augmented-wave (PAW) [14] pseudopotentials for all the atomic species involved;  $f$  electrons of the RE atoms are considered as part of the core. Convergence of the relaxed structural parameters was reached using 550 eV as energy cutoff. Integration of the irreducible Brillouin zone was performed considering shells up to (14, 14, 2) within the Monkhorst and Pack scheme [15]. The presence of Te vacancies was studied using supercells containing up to 52 atoms. All the structures considered were fully relaxed following the *ab initio* calculated forces, optimizing the cell shape to make the stress tensor vanish (up to 0.2 kbar) and converging total energy to less than 0.1 meV/atom. Fermi surfaces and nesting functions are defined, respectively, as

$$FS(\mathbf{k}) = \sum_n \tilde{\delta}(\epsilon_{n\mathbf{k}}) w_{n\mathbf{k}} \quad (1)$$

and

$$N(\mathbf{q}) = \sum_{n\mathbf{k}, n'\mathbf{k}'} \tilde{\delta}(\epsilon_{n\mathbf{k}}) \tilde{\delta}(\epsilon_{n'\mathbf{k}'}) w_{n\mathbf{k}} w_{n'\mathbf{k}'} \delta(\mathbf{q} - \mathbf{k} + \mathbf{k}'), \quad (2)$$

where  $\epsilon_{n\mathbf{k}}$  are the Kohn-Sham eigenvalues,  $n$  is the band index, and  $\mathbf{k}$  is the  $k$  point.  $\tilde{\delta}$  is a numerical approximation of a  $\delta$  function, here taken as a 4 mRy wide step function.  $w_{n\mathbf{k}}$  are band and  $k$ -point weights that account for symmetry and normalization but also for the unfolding procedure used in this work (see Ref. [10,16] for further details). To converge the above expressions, eigenvalues were calculated on much larger grids (64, 64, 1) and interpolated up to (400, 400, 20) points in the Brillouin zone.

## III. THEORETICAL CHARACTERIZATION OF $\text{RE}_4\text{Fe}_2\text{As}_2\text{Te}_{1-x}\text{O}_4$

We present in this section a complete DFT-GGA characterization of this 42214 system, for RE = Pr, Sm, and Gd and including the effect of Te vacancies, pressure, and O  $\rightarrow$  F substitutional doping, in line with the samples and experiments reported so far [7,8]. The limits and predictive power of DFT-GGA were extensively investigated in the last few years and, although its predictions on Fe-based superconductors show some deviations from experiments (for example, overestimation of the magnetic stability and renormalization of the electronic bands), it allows us to properly describe chemical trends, doping effects, Fermi surface topologies, pressure effects, and large unit cells being de-facto the starting point for more advanced and precise computational approaches.

### A. Structural and magnetic properties

The prediction of the lattice parameters were done performing the structural relaxation in the nonmagnetic and on two candidate (and competitive) antiferromagnetic arrangements: the checkerboard phase (AFM1) with antiparallel Fe spins along both the in-plane axes, and the stripe collinear phase (AFM2) with Fe moments parallel along the in-plane diagonals of the 2-Fe unit cell [10]. As discussed in Ref. [10] calculations of a possible bicollinear stripe phase in these materials did not give stable self-consistent solutions of the Kohn-Sham equations and always converged to the nonmagnetic phase, confirming that occurrence of such magnetic order is only found, within DFT, in the 11 FeTe compound [17,18].

Similarly to the pure compounds [10], AFM2 is predicted as the ground state phase for all three REs and in Fig. 1 and Table I, we report the corresponding magnetic and structural properties. We point out that the magnetic properties of 42214 compounds are not yet being experimentally studied and, in this respect, low temperature experiments would be highly desirable to ascertain whether the 42214 samples undergo the structural and magnetic phase transition, as found in other families of pnictides.

We find that the magnetic stability is affected by the presence of Te vacancies; Fig. 1(a) illustrates the stability of the AFM2 phase that depends on the RE atom as well as on the Te content. At fixed Te content, RE substitution (moving from Pr to Gd) favors the instability of the magnetic ground state phase: the reduction of the RE covalent radius induces a chemical internal pressure which locally shrinks the volume and raises the As height from the Fe planes; this last effect has been often related to enhanced correlation effects and smaller effective magnetic exchange couplings [19]. On the other hand, keeping the RE fixed, Te vacancies lower the stability of the AFM2 ground state phase with respect to the nonmagnetic phase. Despite the fact that substitution of the RE element induces larger structural effects than those due to Te vacancies [10], both weaken, up to the same order of magnitude, the stability of the long-range magnetic order.

At the same time, the Fe-magnetic moment ( $\mu_{\text{Fe}}$ ) decreases with the contraction of the RE covalent radius but increases with the concentration of Te vacancies [see Fig. 1(b)]: the size of Fe-magnetic moment is not correlated with the stability

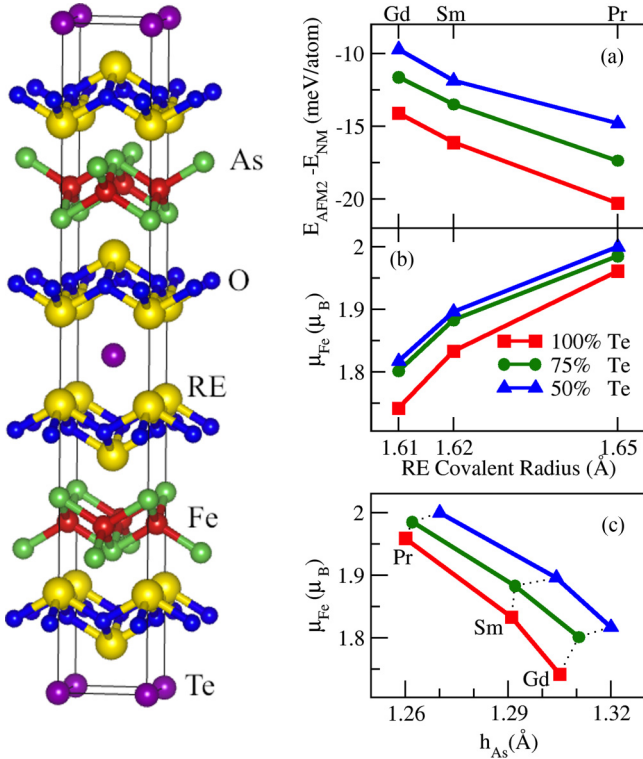


FIG. 1. Left: Crystal structure of the 42214 compounds: 3D view of the tetragonal cell. Here red, green, yellow, blue, and purple circles represent Fe, As, RE, O, and Te atoms, respectively. Right: (a) Stability of the AFM2 ground state phase and (b) relative magnetic moment  $\mu_{\text{Fe}}$  as a function of the RE covalent radius ( $R = 1.61, 1.62, 1.65 \text{ \AA}$  for Gd, Sm, and Pr, respectively) and at different Te content ( $1 - x = 50\%, 75\%$ , and  $100\%$ ). (c) Dependence of the Fe-magnetic moment ( $\mu_{\text{Fe}}$ ) on the As height ( $h_{\text{As}}$ ),

of the AFM2 phase. To highlight this effect we illustrate in Fig. 1(c) the variability of the Fe-magnetic moment ( $\mu_{\text{Fe}}$ ) in the 42214 compounds as a function of RE element, Te content ( $1 - x$ ), and As height ( $h_{\text{As}}$ ). It emerges that, at the Te contents considered, the Fe-magnetic moment is always lower for RE = Gd, while it is always larger for RE = Pr. Indeed, reduction of the RE covalent radius implies an increase of the As height toward the *optimal* empirical value for superconductivity ( $h_{\text{As}} \simeq 1.38 \text{ \AA}$  [20]) joined by a decrease of the Fe-magnetic moment (up to 11%) which weakens the stability of the AFM2 phase. However, fixing the RE element, introduction of Te vacancies determines, likewise,

TABLE I. Structural parameters [lattice parameters ( $a, b, c$ ), As-height ( $h_{\text{As}}$ ), and volume ( $V$ )] at 0 pressure in the  $\text{Sm}_4\text{Fe}_2\text{As}_2\text{Te}_{1-x}\text{O}_4$  compounds for different Te contents ( $1 - x = 50\%, 75\%$ , and  $100\%$ ).

	50% Te	75% Te	100% Te
$a(\text{\AA})$	4.00	4.01	4.01
$b(\text{\AA})$	3.98	3.98	3.98
$c(\text{\AA})$	29.45	29.52	29.68
$h_{\text{As}}(\text{\AA})$	1.304	1.292	1.291
$V(\text{\AA}^3)$	468.84	471.13	473.69

an increase of the As height, which favors the magnetic instabilities, but also a larger Fe-magnetic moment (up to 4%).

These results clearly highlight that not only RE-element substitution but also Te content is an effective tool to modify the structural ( $h_{\text{As}}$ ) and magnetic parameters ( $\mu_{\text{Fe}}$  and AFM2 phase stability), which are key parameters playing a key role for the transition to the superconductive phase in the 42214 compounds. Theoretical understanding of the spin-fluctuation mechanism of superconductivity [21–30], including recent *ab initio* types of theories [31–34], indicate that while superconductivity could always occur at the onset of a magnetic instability due to the divergence of the magnetic response function,  $T_C$  can be very different depending on how the transition actually occurs and, therefore, on the features of the magnetic susceptibility [22,33,35]. The availability of multiple tuning leverages, as in this case, is therefore very positive in view of maximizing the transition temperature.

## B. Electronic properties

The possibility of superconductivity induced by a magnetic fluctuation mechanism, or in general by a repulsive interaction, poses constraints on the shape of the Fermi surface which can sustain these pairing mechanisms (or more specifically on the properties of the single particle excitation spectrum in the energy scale of the pairing bosonic field [21,22,26,36]).

In view of this basic concept, we now investigate how Te vacancies affect the electronic properties of the 42214 materials. Being mostly interested on the connection to superconductivity we study the nonmagnetic electronic configuration. As an example, we concentrate on the Gd-based compound which seems to be the most promising from the point of view of superconducting properties and consider both the case of 75% Te concentration, a value which is not far away from the Te contents experimentally achieved, and of 50% Te concentration.

As we can see from Figs. 2(a) and 2(b), in the fully stoichiometric compound, Te-related states are located between 3.0 and 0.5 eV below the Fermi level (set to zero in the figure). Te vacancies induce a splitting of these states into two sets: one moving at about +1.5 eV and one remaining localized at  $-3 \text{ eV}$ . The effect is local: at 75% of doping (1 Te vacancy per unit cell, in our supercell) this occurs only for the states originating from Te atoms belonging to the plane in which the vacancy is contained, while the other Te atoms are scarcely affected. Therefore, Te vacancies produce two inequivalent Te sites: one chemically indistinguishable from the undoped case [compare black lines in Figs. 2(b) and 2(c)], and one strongly affected by the vacancy [gray line Fig. 2(c)]. This is confirmed considering the 50% Te vacancy case (modeled as one Te vacancy per plane): here all the Te states are modified with respect to the parent (undoped) compound [compare gray line in Figs. 2(c) and 2(d)].

In order to interpret the low energy electronic band structure of the defective supercell, rather complex due to Brillouin-zone folding effects, we adopt a computational procedure (see Refs. [10,16]) to unfold the band structure into the 1-Fe Brillouin zone, where hole and electron pockets (together with their nesting properties) can be clearly distinguished [22].

The calculated band structures projected on the iron atoms and unfolded into the 1Fe bct unit cell for the stoichiometric

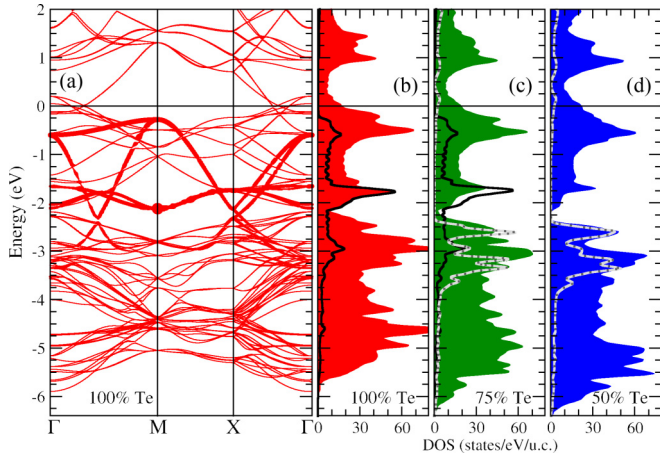


FIG. 2. (a) Band structure projected on the  $p$  orbitals of Te calculated for  $\text{Gd}_4\text{Fe}_2\text{As}_2\text{TeO}_4$  in the nonmagnetic state. (b)–(d) Density of electronic states for  $\text{Gd}_4\text{Fe}_2\text{As}_2\text{Te}_{1-x}\text{O}_4$ , respectively, for  $1-x = 100\%$ ,  $75\%$ , and  $50\%$ , respectively. The shaded area (red, green, and blue) is the total density of states. Black and dashed-gray lines are the 1-Te projected density of states. Black is used for Te atoms belonging to a fully occupied Te layer; dashed gray for Te atoms in a layer with Te vacancies (50%). All 1-Te projections are multiplied by a factor of 20 for plotting convenience.

and defective Gd-based compounds are shown in Fig. 3 (panels from top to bottom with increasing vacancy concentration). We can now clearly see that Te vacancies act as electron dopants, almost rigidly shifting the Fermi level towards higher energy. In the defective compounds, Te- $\sigma$  and dangling bonds surrounding the vacancy, together with out-of-plane  $\pi$ -like bonds with adjacent RE-O planes, contribute free carriers to the Fe-As planes. This last mechanism is revealed by a nonvanishing Te  $p$ -like contribution to the density of states in

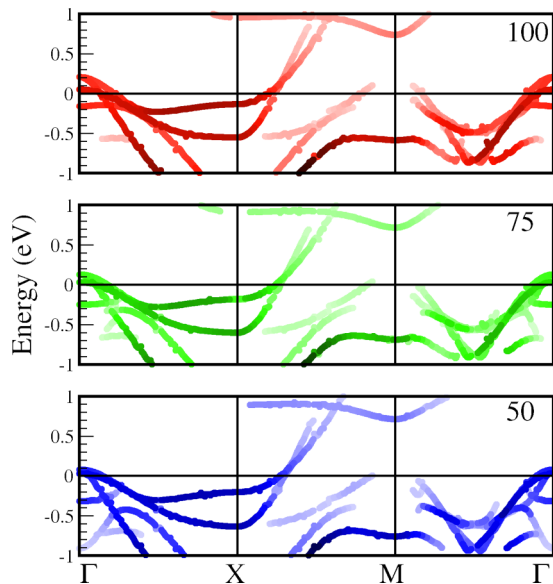


FIG. 3. Band structures projected on the basal plane of the 1Fe bct unit cell for the  $\text{Gd}_4\text{Fe}_2\text{As}_2\text{Te}_{1-x}\text{O}_4$  ( $1-x = 100\%$ ,  $75\%$ , and  $50\%$  from top to bottom panels, respectively) calculated in the nonmagnetic state and at their respective equilibrium structure.

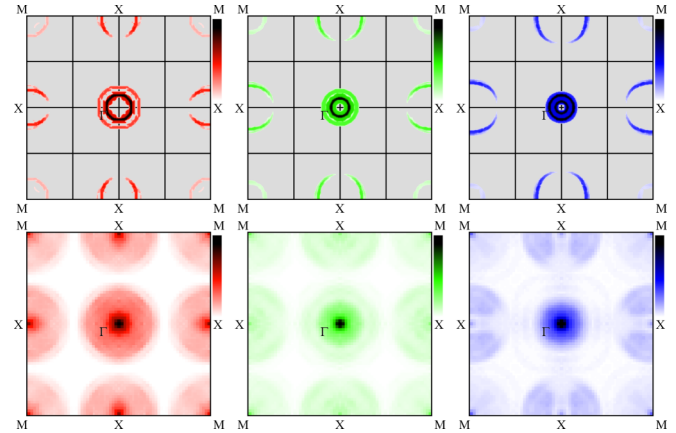


FIG. 4. Fermi surface (top panels) and nesting function (bottom panels) projected on the basal plane of the 1Fe bct unit cell for  $\text{Gd}_4\text{Fe}_2\text{As}_2\text{Te}_{1-x}\text{O}_4$  ( $1-x = 100\%$ ,  $75\%$ , and  $50\%$ , panels from left to right, respectively) at their respective equilibrium structure. The color intensity is proportional to the value of the nesting function normalized to its value at the zone center.

proximity of the Fermi level (not shown). In addition, doping affects differently Fe- $d$  states at the Fermi level and cannot be considered as rigid: in fact,  $d_{xz,yz}$  holes are shifted more than  $d_{x^2-y^2}$  and  $d_{z^2}$  states.

In Fig. 4 (top panels) we report the cut of the Fermi surface (FS) in the  $\Gamma$ - $X$ - $M$  plane of the 1Fe unit-cell Brillouin zone, at different vacancy concentrations. We observe that the zone center pockets (hole FS) shrink and those at  $X$  (electron FS) become larger. These same effects reflect on the nesting function (Fig. 4, bottom panels) which, in a first-principles theory of spin-mediated effective interaction [31,33], plays a fundamental role on the origin of superconducting instability: the intensity of the nesting function is dramatically weakened increasing Te vacancies and the allowed nesting vectors close to  $X$  are strongly reduced in number (the colored area sensibly shrinks upon Te deficiency). All these evidences point to the same conclusion: Te vacancies enlarge electronlike and shrink holelike FS features, resulting in an overall lowering of nesting properties; this weakens long-range magnetic order (AFM2) stability and enhances magnetic spin fluctuations which could possibly contribute to the onset of superconductivity. Although, at the moment, theoretical understanding of iron-based superconductors is still far from being complete and it is not clear how the superconducting critical temperature can be controlled, we found that Te vacancies are able to significantly affect the structure of the Fermi surface still without changing its topology, producing a fine tuning of the nesting properties of electron and hole bands.

### C. Pressure effects

Pressure has been shown to induce superconductivity and to increase the superconducting critical temperature [37–41] in iron-based superconductors strongly modifying the electronic and magnetic properties of the materials [39]. Substitution of RE atoms in the 42214 compounds may, actually, be interpreted as mainly a chemical pressure effect, although largely nonhydrostatic [10,42]. We thus extend our investigations and

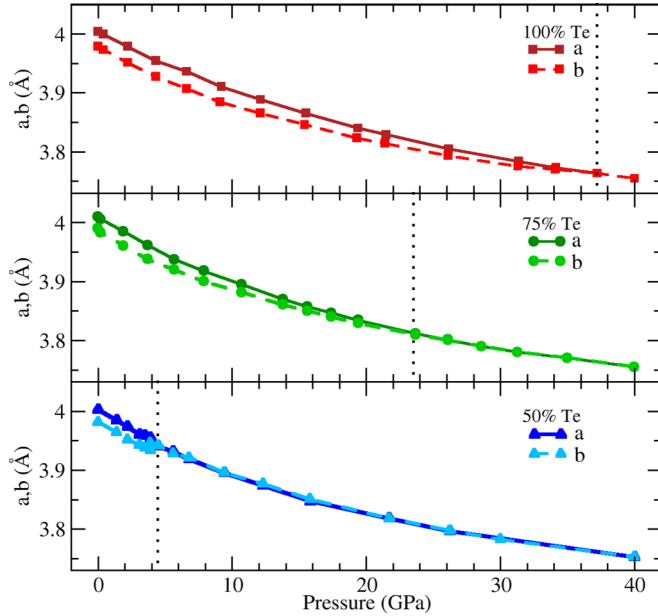


FIG. 5. Structural orthorhombic in-plane parameters ( $a, b$ ) of  $\text{Sm}_4\text{Fe}_2\text{As}_2\text{Te}_{1-x}\text{O}_4$  compounds as a function of external hydrostatic pressure at different Te concentrations ( $1 - x = 50\%$ ,  $75\%$ , and  $100\%$ ).

predict the effect of high hydrostatic pressure on the physical properties of 42214 compounds.

Since trends are only weakly dependent on the RE (with RE = Pr and Gd), we will base our discussion on the Sm compound  $\text{Sm}_4\text{Fe}_2\text{As}_2\text{Te}_{1-x}\text{O}_4$ , considering different Te content ( $1 - x = 50\%$ ,  $75\%$ , and  $100\%$ ). At all doping, we predict the occurrence of an orthorhombic to tetragonal phase transition upon compression, clearly seen in the pressure dependence of the  $a$  and  $b$  lattice parameters in Fig. 5. The structural phase transition occurs at about 37 GPa in the stoichiometric compound and decreases, thanks to Te vacancies, to only 4 GPa at 50% of Te content (refer to Table II for the full structural data at the transition). This result is consistent with the discussion in Sec. III A where it was shown how Te vacancies lower the stability of the long-range magnetic order favoring a nonmagnetic solution. Although the transition pressure predicted within DFT-GGA may differ from the actual experimental one [23], the qualitative (and in many cases quantitative) picture should remain valid [39,40].

TABLE II. Structural parameters [lattice parameters ( $a, b, c$ ), As height ( $h_{\text{As}}$ ), and volume ( $V$ )] at the critical pressure values, where transition from the orthorhombic to the tetragonal phase occurs in the  $\text{Sm}_4\text{Fe}_2\text{As}_2\text{Te}_{1-x}\text{O}_4$  compounds at different Te contents ( $1 - x = 50\%$ ,  $75\%$ , and  $100\%$ ).

	50% Te	75% Te	100% Te
$a_{\text{crit}}, b_{\text{crit}}(\text{\AA})$	3.94	3.81	3.76
$c_{\text{crit}}(\text{\AA})$	28.32	26.51	25.82
$h_{\text{As}}(\text{\AA})$	1.27	1.22	1.20
$V_{\text{crit}}(\text{\AA}^3)$	439.63	384.82	365.03
$P_{\text{crit}}(\text{GPa})$	4.53	24.00	37.22

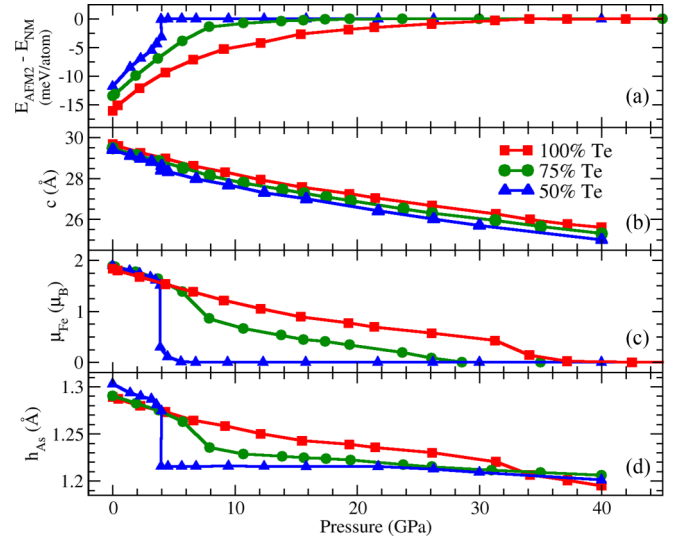


FIG. 6. Pressure dependence of the structural and magnetic properties of  $\text{Sm}_4\text{Fe}_2\text{As}_2\text{Te}_{1-x}\text{O}_4$  compounds at different Te contents ( $1 - x = 50\%$  red,  $75\%$  green, and  $100\%$  blue). (a) Stability of the AFM solution as compared to the nonmagnetic calculation; (b) lattice structural  $c$  parameter; (c) average magnetic moment at the iron site  $\mu_{\text{Fe}}$ ; and (d) average height of the As atom with respect to the iron plane.

In DFT based methods, the orthorhombic distortion is induced by the spin density wave and, thus, does not describe a possible nematic phase which however can exist above the Néel temperature. The tetragonal phase transition is thus accompanied by a drop to zero of the Fe magnetic moment [Fig. 6(c)], perfectly matched by an adjustment of the As position [Fig. 6(d)]. The magnetic trend shows that, while the transition in the stoichiometric system is continuous (second order), it becomes discontinuous upon doping and is clearly of first order in the system with 50% Te vacancies: this can be seen in the behavior of the magnetic moment Fig. 6(c) and directly from the energetics in Fig. 6(a).

The first order transition is also seen in the pressure dependence of  $c$  lattice constant [Fig. 6(b)], that is induced by the collapse of the As-Fe planes, and in turn by the magnetic transition. Such a small structural collapse may remind us of a similar phenomena observed in the 122 family (see for example [43]); however, in this case the effect is significantly smaller since is not originating from a change in chemical coordination and the formation of an As-As interlayer bond.

The role of Te vacancies, significant already at ambient pressure, is fully exploited upon compression: vacancies shift the AFM  $\rightarrow$  NM transition to lower pressures (as expected from the results of Sec. III A), but also affect the way the phase transition itself occurs. Superconducting theories considering spin-fluctuation mechanisms [21,22,24,26,31,44] clearly indicate that this is the main aspect setting the stability of the SC phase and the value of  $T_c$ .

#### D. Fluorine doping

In addition to Te vacancies, we consider the effect of F doping, i.e., F substituting on the oxygen site. Fluorine-doped

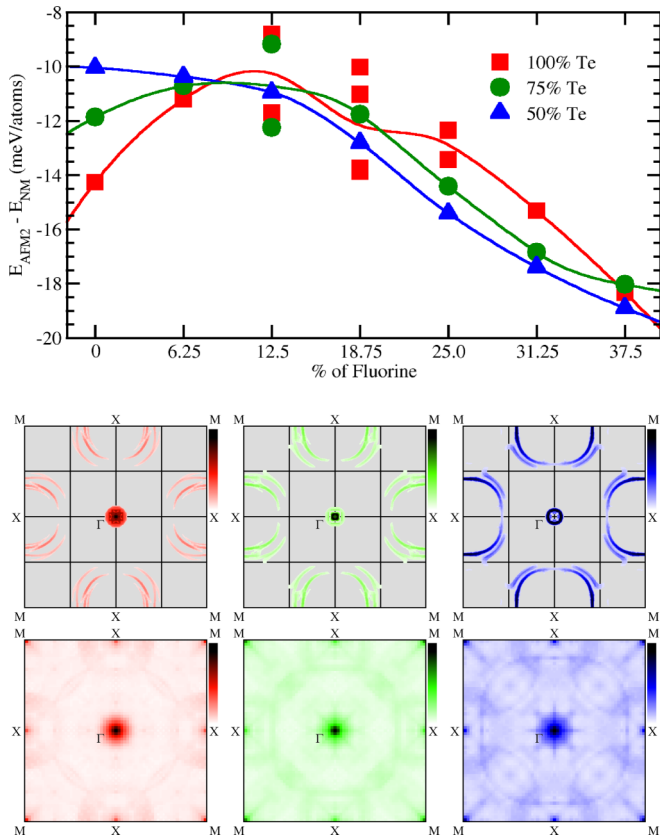


FIG. 7. Top panel: Stability of the magnetic ground state (AFM2) for the  $Gd_4Fe_2As_2Te_{1-x}O_{4-y}F_y$  as a function of F concentration ( $y$ ) at different Te contents ( $1-x = 100\%$ ,  $75\%$ , and  $50\%$ ). Multiple data at fixed concentration indicate results for different relative position of dopants. Lines are guide to the eye. Central panels: Fermi surfaces at 25% of F doping and different Te contents ( $1-x = 100\%$ ,  $75\%$ , and  $50\%$  panels from left to right). Bottom panels: Corresponding nesting function.

crystals 42214 were studied by single crystal x-ray diffraction experiments and resistivity [8]. However, since the experimental characterization of F doped samples is sparse, it is difficult to extract clear trends from these measurements. It certainly emerges that fluorine doping has a significant effect on  $T_C$  inducing a significant enhancement [8]. Present calculations (in agreement with Ref. [10]) show that, being substitutional, F induces minor modifications to the lattice parameters. However, we do see a significant effect on the magnetic stability, as shown in Fig. 7. This effect strongly depends on the spatial distributions of fluorine atoms, as shown in Fig. 7 where results for different doping sites are indicated as multiple data at the same F concentration. However, since doping will be stochastically distributed on the sample, the expected trend will be close to an average of the various configurations considered. Despite the sparse data resulting from the different relative position of the dopants, we observe a clear trend: F doping scarcely affects the stability of the magnetic phase up to about 20%; however, further increase of F content induces a clear stabilization of the magnetic.

The stabilization energies are of the same order of those related to RE substitution and Te vacancies (cf. Fig. 1), so the

three mechanisms could be possibly combined to obtain a fine tuning of the desired properties.

As expected, F substitution results in an electron doping, filling the hole pocket at the zone center, as seen from Fig. 7 (central panels). At 25% F concentration, the hole pocket has almost disappeared while the electron one is enlarged. The nesting features (see Fig. 7) are consequently reduced. However, as highlighted in Refs. [22,23,44] this strongly asymmetric configuration may still be compatible with an  $s\pm$  symmetry for the superconducting order parameter, but, due to the size of the electronic pocket, a  $d$ -wave symmetry may also be possible.

#### IV. $RE_4Fe_2As_2Se_{1-x}O_4$ : COULD $Te \rightarrow Se$ SUBSTITUTION LEAD TO HIGHER $T_C$ VALUES?

To go beyond the present experimental scenario and hopefully stimulate further work on this rich 42214 family, we present here the computational predictions of  $RE_4Fe_2As_2Se_{1-x}O_4$  ( $RE = Pr, Sm, \text{ and } Gd$ ) where Te atoms are substituted by Se.

Figure 8 reports the most relevant structural and magnetic properties, namely the As height with respect to the Fe layers ( $h_{As}$ ), the Fe magnetic moment ( $\mu_{Fe}$ ), and the stability of the AFM2 ground state phase with respect to the nonmagnetic one ( $E_{AF2M} - E_{NM}$ ) as a function of Se concentration and RE. To make the comparison easier, we also report the corresponding values for the Te compounds discussed in the previous part of this paper. These results show that substitution of Te with Se atoms, having smaller covalent radius, determines

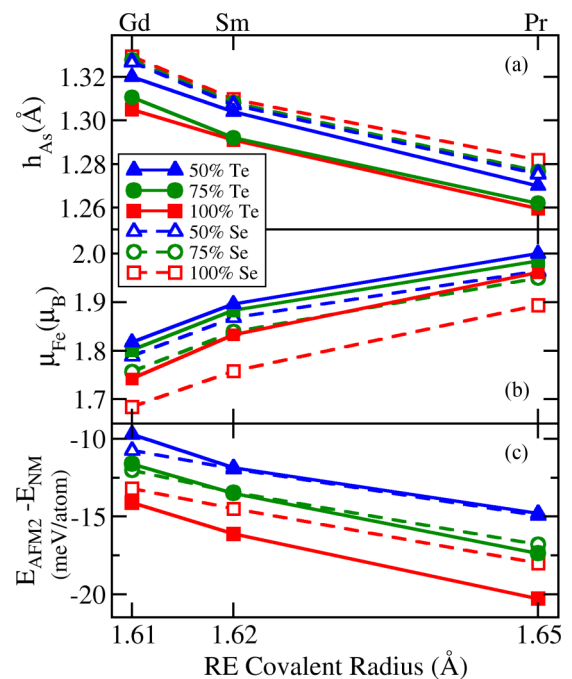


FIG. 8. (a) As height, (b) Fe magnetic moment, and (c) stability of the AFM2 ground state phase with respect to the nonmagnetic one, as a function of Se concentration (dashed line) in the  $RE_4Fe_2As_2Se_{1-x}O_4$  ( $RE = Pr, Sm, \text{ and } Gd$ ) compounds. The same physical quantities in  $RE_4Fe_2As_2Te_{1-x}O_4$  ( $RE = Pr, Sm, \text{ and } Gd$ ) materials are reported as a function of the Te concentration (solid lines), for comparison.

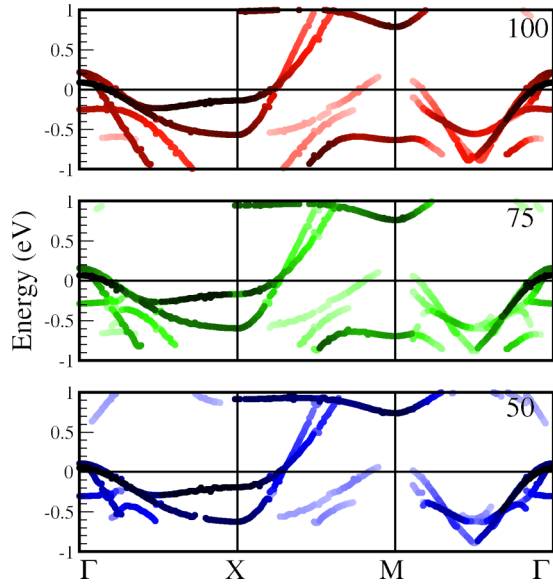


FIG. 9. Band structure projected on Fe atoms of the 1Fe bct unit cell for the  $\text{Gd}_4\text{Fe}_2\text{As}_2\text{Se}_{1-x}\text{O}_4$  at different Se content ( $1 - x = 100\%$ ,  $75\%$ , and  $50\%$ , top, central, and bottom panels, respectively) calculated in the nonmagnetic state and at their respective equilibrium structure.

in general large effect and, interestingly, a systematic increase of the As height. At the same time the magnetic moment as well as the stability of the magnetic phase is reduced due enhanced correlation effects and smaller effective magnetic couplings [19].

In Figs. 9 and 10 we report the results for the electronic properties.

The similarities of the Fermi surface features with those of the Te-based compounds (cf. Figs. 3 and 4) are striking: despite the structural changes induced by Se substitution the states at the Fermi level as well as the nesting function are affected only to a minor extent.

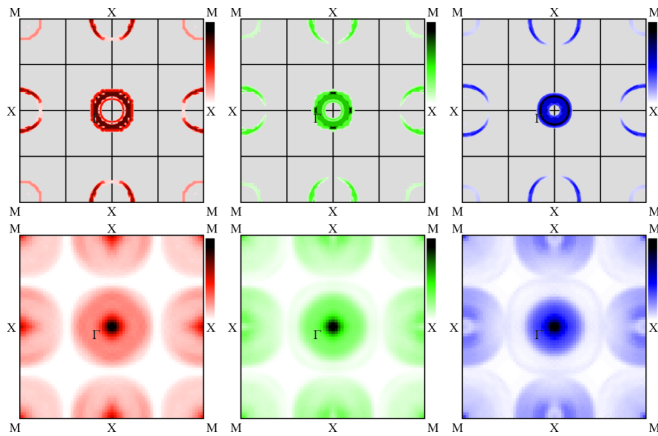


FIG. 10. Fermi surface (top panels) and nesting function (bottom panels) projected on the basal plane of the 1Fe bct unit cell for  $\text{Gd}_4\text{Fe}_2\text{As}_2\text{Se}_{1-x}\text{O}_4$  for different Se content ( $1 - x = 100\%$ ,  $75\%$ , and  $50\%$ , from left to right panels, respectively) at their respective equilibrium structure. The color intensity is proportional to the value of the nesting function normalized to its value at the zone center.

Although great accomplishments have been recently reached along this line, it is presently impossible to obtain a completely parameter-free prediction of the superconducting properties [32,34] of this system or other Fe-based superconductors. In this respect Se substitution increases  $h_{\text{As}}$  probably increasing correlation effects, and lowers the stability of the magnetic phase, giving an indication that the Se family may actually have a higher critical temperature than the Te one.

## V. CONCLUSIONS

To summarize, in this work we have presented a systematic first-principles study that allows us to better understand the main mechanisms which drive the sought-after 42214 material properties measured by Katrych and co-workers [7,8] and that completes our previous theoretical work on the 42214 pure stoichiometric compounds [10]. In particular, the role of Te atoms and of their vacancies on the physical properties of  $\text{RE}_4\text{Fe}_2\text{As}_2\text{Te}_{1-x}\text{O}_4$  ( $\text{RE} = \text{Pr}, \text{Sm}, \text{and Gd}$ ) materials is analyzed and discussed: it emerges that the effect of the Te vacancies is much more dramatic than that of RE substitution [10]. On one hand, Te atoms are fundamental for the structural stability of the compounds, on the other hand, Te vacancies play a crucial role for a possible transition to the superconducting phase. In fact, we find that: (i) the stripe collinear antiferromagnetic phase (AFM2) is the ground state phase for the 42214 compounds independently on the concentration of Te concentration ( $1 - x = 50\%$ ,  $75\%$ , and  $100\%$ ), however, its stability is lowered as the number of Te vacancies increases; (ii) the presence of Te vacancies contributes to enhance the magnetic instability through a combined structural and electronic effect (higher As height, lower energy difference between nonmagnetic and AFM2 state, charge transfer in FeAs layers, lower nesting function) that may favor the possible onset of the superconducting state; (iii) external pressure induces the vanishing of the magnetic order with a transition to the tetragonal phase which changes from first to second order as the number of Te vacancies increases; (iv) in analogy with Te vacancies, the chemical substitution of oxygen with fluorine atoms is shown to act as charge dopant, lowering the carrier number at the Fermi level (reduced Fermi surface and nesting function features) and decreasing the magnetic order stability that favors the transition to the superconducting phase; and (v) new compounds characterized by intercalated Se layers instead of Te atoms are promising materials that present important similarities with the 42214 compounds: at the same time, they exhibit higher As heights and higher instability of the magnetic phase that may allow us to further increase the superconducting critical temperature.

## ACKNOWLEDGMENTS

This work was supported by SUPER-IRON (EU-FP7 grant), PriN-2012 (IT-MIUR grant), and HPC ISCR-A-B and ISCR-A-C grants at Cineca HPC center. F. Bucci acknowledges the ERASMUS program at Università degli Studi dell'Aquila for financial support during his stay at Max Planck Institute for Microstructure Physics. The authors acknowledge S. Katrych and J. Katpinski for pointing out the scientific topic. F.B. thanks C. Tresca for useful discussions.

- [1] H. Takahashi, K. Igawa, K. Arii, Y. Kamihara, H. Masahiro, and H. Hosono, *Nature (London)* **453**, 376 (2008).
- [2] M. Rotter, M. Tegel, and D. Johrendt, *Phys. Rev. Lett.* **101**, 107006 (2008).
- [3] Y. Kamihara, H. Hiramatsu, M. Hirano, R. Kawamura, H. Yanagi, T. Kamiya, and H. Hosono, *J. Am. Chem. Soc.* **128**, 10012 (2006).
- [4] G. R. Stewart, *Rev. Mod. Phys.* **83**, 1589 (2011).
- [5] H. Hosono and K. Kuroki, *Physica C* **514**, 399 (2015), superconducting Materials: Conventional, Unconventional and Undetermined .
- [6] J. H. Tapp, Z. Tang, B. Lv, K. Sasmal, B. Lorenz, P. C. W. Chu, and A. M. Guloy, *Phys. Rev. B* **78**, 060505 (2008).
- [7] S. Katrych, K. Rogacki, A. Pisoni, S. Bosma, S. Weyeneth, R. Gaal, N. D. Zhigadlo, J. Karpinski, and L. Forró, *Phys. Rev. B* **87**, 180508 (2013).
- [8] S. Katrych, A. Pisoni, S. Bosma, S. Weyeneth, N. D. Zhigadlo, R. Gaal, J. Karpinski, and L. Forró, *Phys. Rev. B* **89**, 024518 (2014).
- [9] A. Pisoni, P. Szirmai, S. Katrych, B. Náfrádi, R. Gaál, J. Karpinski, and L. Forró, *Phys. Rev. B* **93**, 094519 (2016).
- [10] F. Bucci, A. Sanna, A. Continenza, S. Katrych, J. Karpinski, E. K. U. Gross, and G. Profeta, *Phys. Rev. B* **93**, 024518 (2016).
- [11] G. Kresse and J. Furthmüller, *Phys. Rev. B* **54**, 11169 (1996).
- [12] G. Kresse and J. Furthmüller, *Comput. Mater. Sci.* **6**, 15 (1996).
- [13] J. P. Perdew, K. Burke, and M. Ernzerhof, *Phys. Rev. Lett.* **77**, 3865 (1996).
- [14] P. E. Blöchl, *Phys. Rev. B* **50**, 17953 (1994).
- [15] H. J. Monkhorst and J. D. Pack, *Phys. Rev. B* **13**, 5188 (1976).
- [16] M. W. Haverkort, I. S. Elfimov, and G. A. Sawatzky, [arXiv:1109.4036](https://arxiv.org/abs/1109.4036).
- [17] M. Monni, F. Bernardini, G. Profeta, and S. Massidda, *Phys. Rev. B* **87**, 094516 (2013).
- [18] C. Tresca, F. Ricci, and G. Profeta, *2D Mater.* **2**, 015001 (2014).
- [19] C. Zhang, L. W. Harriger, Z. Yin, W. Lv, M. Wang, G. Tan, Y. Song, D. L. Abernathy, W. Tian, T. Egami, K. Haule, G. Kotliar, and P. Dai, *Phys. Rev. Lett.* **112**, 217202 (2014).
- [20] Y. Mizuguchi, Y. Hara, K. Deguchi, S. Tsuda, T. Yamaguchi, K. Takeda, H. Kotegawa, H. Tou, and Y. Takano, *Supercond. Sci. Technol.* **23**, 054013 (2010).
- [21] D. Manske, *Theory of Unconventional Superconductors, Cooper-Pairing Mediated by Spin Excitations* (Springer, Berlin, 2004).
- [22] I. I. Mazin, D. J. Singh, M. D. Johannes, and M. H. Du, *Phys. Rev. Lett.* **101**, 057003 (2008).
- [23] I. I. Mazin, *Nature (London)* **464**, 183 (2010).
- [24] I. I. Mazin and M. D. Johannes, *Nat. Phys.* **5**, 141 (2009).
- [25] P. J. Hirschfeld, M. M. Korshunov, and I. I. Mazin, *Rep. Prog. Phys.* **74**, 124508 (2011).
- [26] D. J. Scalapino, *Rev. Mod. Phys.* **84**, 1383 (2012).
- [27] E. Dagotto, A. Moreo, A. Nicholson, Q. Luo, S. Liang, and X. Zhang, *Frontiers Phys.* **6**, 379 (2011).
- [28] T. Li, *J. Phys.: Condens. Matter* **20**, 425203 (2008).
- [29] J. Lorenzana, G. Seibold, C. Ortix, and M. Grilli, *Phys. Rev. Lett.* **101**, 186402 (2008).
- [30] M. Daghofer, A. Moreo, J. A. Riera, E. Arrigoni, D. J. Scalapino, and E. Dagotto, *Phys. Rev. Lett.* **101**, 237004 (2008).
- [31] F. Essenberg, A. Sanna, A. Linscheid, F. Tandetzyk, G. Profeta, P. Cudazzo, and E. K. U. Gross, *Phys. Rev. B* **90**, 214504 (2014).
- [32] F. Essenberg, A. Sanna, P. Buczek, A. Ernst, L. Sandratskii, and E. K. U. Gross, *Phys. Rev. B* **94**, 014503 (2016).
- [33] F. Essenberg, P. Buczek, A. Ernst, L. Sandratskii, and E. K. U. Gross, *Phys. Rev. B* **86**, 060412 (2012).
- [34] J. Lischner, T. Bazhurov, A. H. MacDonald, M. L. Cohen, and S. G. Louie, *Phys. Rev. B* **91**, 020502 (2015).
- [35] M. Monni, F. Bernardini, G. Profeta, A. Sanna, S. Sharma, J. K. Dewhurst, C. Bersier, A. Continenza, E. K. U. Gross, and S. Massidda, *Phys. Rev. B* **81**, 104503 (2010).
- [36] C. C. Tsuei and J. R. Kirtley, *Rev. Mod. Phys.* **72**, 969 (2000).
- [37] E. Colombier, S. L. Bud'ko, N. Ni, and P. C. Canfield, *Phys. Rev. B* **79**, 224518 (2009).
- [38] T. Yamazaki, N. Takeshita, R. Kobayashi, H. Fukazawa, Y. Kohori, K. Kihou, C.-H. Lee, H. Kito, A. Iyo, and H. Eisaki, *Phys. Rev. B* **81**, 224511 (2010).
- [39] N. Colonna, G. Profeta, and A. Continenza, *Phys. Rev. B* **83**, 224526 (2011).
- [40] N. Colonna, G. Profeta, A. Continenza, and S. Massidda, *Phys. Rev. B* **83**, 094529 (2011).
- [41] J. Zhao, H. Liu, L. Ehm, D. Dong, Z. Chen, Q. Liu, W. Hu, N. Wang, and C. Jin, *Inorg. Chem.* **52**, 8067 (2013).
- [42] W. J. Duncan, O. P. Welzel, C. Harrison, X. F. Wang, X. H. Chen, F. M. Grosche, and P. G. Niklowitz, *J. Phys.: Condens. Matter* **22**, 052201 (2010).
- [43] A. Sanna, G. Profeta, S. Massidda, and E. K. U. Gross, *Phys. Rev. B* **86**, 014507 (2012).
- [44] E. Bascones, B. Valenzuela, and M. J. Calderón, *C. R. Phys.* **17**, 36 (2016), iron-based superconductors.